Available online at www.sciencedirect.com
SCIENCE DIRECT
Journal of Magnetic Resonance 178 (2006) 288–296
JMR Journal of Magnetic Resonance
www.elsevier.com/locate/jmr

Sectoral sampling in centric-scan SPRITE magnetic resonance imaging

Alexandre A. Khrapitchev, Benedict Newling, Bruce J. Balcom *

Department of Physics, University of New Brunswick, P.O. Box 4400, Fredericton, NB, Canada E3B 5A3

Received 30 August 2005; revised 9 October 2005
Available online 10 November 2005

Abstract

A new approach to the construction of *k*-space trajectories for centric-scan SPRITE in both 2D and 3D is presented. All benefits of previous SPRITE methods are retained, most importantly the ability to image objects with short T_2^*. This new approach gives more flexibility in the choice of number of interleaves with points more evenly distributed across *k*-space. All these improvements positively contribute to image quality and resolution, which can be also traded off against experimental speed. Sectoral sampling will have significant benefits for magnetisation preparation contrast imaging.
© 2005 Elsevier Inc. All rights reserved.

Keywords: MRI; Short T_2^*; SPRITE; Materials; Sectoral trajectory; Pure phase encoding; Single point imaging

1. Introduction

The principal limits for conventional MRI methods, applied to natural science, are the transverse lifetimes T_2^* and T_2 of the MRI signal, which are sufficiently short in solids, semi-solids, liquid crystals, and many gases, to make traditional MRI challenging or impossible. Single-point imaging (SPI) MRI methods are able to cope with many of these limitations [1]. In conventional MRI, the time evolution of magnetisation is measured in the presence of a constant magnetic field gradient (frequency encoding). In contrast, SPI is a purely phase-encoded technique; magnetisation is sampled at fixed intervals (t_p) after *RF* excitation, but the amplitude of the accompanying magnetic field gradient is varied from *RF* excitation to *RF* excitation. There is current interest in clinical MRI in the imaging of tissues with short signal lifetimes [2] and continued interest in materials MRI. The possibility of using a relatively short t_p makes SPI well-suited to the imaging of substances with T_2^* and $T_2 \ll 1$ ms.

The most generally applicable SPI MRI method is SPRITE (single point ramped imaging with T_1 enhancement) [3]. One of the principal adaptations of SPRITE employs continuously ramped gradients with data acquisition commencing at the centre of *k*-space (Centric Scan SPRITE) [4]. This approach improves the signal-to-noise (S/N) ratio per unit acquisition time, simplifies the image contrast and reduces the gradient duty cycle limitation of previous implementations. SPRITE methods are mostly targeted towards samples with short lifetimes, but they also can be successfully applied in investigations where lifetimes are not a limiting factor.

MRI is a truly non-invasive technique, which is its principal advantage over other imaging modalities, particularly in the study of dynamic systems. Also crucial in such studies, however, is imaging speed. Among materials MRI methods, the SPRITE technique is relatively fast and particularly well suited to the investigation of rapidly evolving systems. However, it is much harder to compare the speed of different methods by acquiring comparable quality images, than it is to fix all other experimental parameters and judge the difference in image quality and resolution. We take the latter approach, bearing in mind that inherent improvements to image quality, can be traded off against other MRI commodities, such as imaging speed.

Image resolution in Centric SPRITE imaging is governed by the balance of T_1, flip angle (*RF* pulse power) and the time between *RF* pulses [5]. In some SPRITE cases, in order to obtain homogeneous excitation of the spin sys-

* Corresponding author. Fax: +1 506 453 4581.
E-mail address: bjb@unb.ca (B.J. Balcom).

1090-7807/$ - see front matter © 2005 Elsevier Inc. All rights reserved.
doi:10.1016/j.jmr.2005.10.006

tem, the duration of the *RF* pulses is also limited by the maximum spectral width of the object ($G_{max} \times$ length of the sample). Therefore, extensive signal averaging may be required to achieve reasonable S/N ratio. For samples with short T_1, the accumulations can be rapid. For materials with long T_1 any requirement for intensive signal averaging will lead to a significant increase in experimental time. We note that the collection of multiple FID data points provides a separate, time-efficient route to signal averaging, in some favourable circumstances [5].

The sample magnetisation may be prepared before imaging by invoking relaxation time or other contrast [6]. However, the magnetisation will evolve towards a dynamic equilibrium, which contains no relation to the preparation, during the readout of k-space [5]. The sample T_1 is once again a critical parameter. In such cases a k-space trajectory divided into shorter parts may be desirable. The average duration of an individual leaf, for a fixed matrix size, depends on the number of leaves. Therefore, it is necessary to have a variety of available sampling strategies, with variable number of leafs, for experiment optimisation with a broad range of sample T_1s [4].

Requiring flexible k-space segmentation ensures a different emphasis for the design of k-space sampling schemes in pure phase encoded imaging compared to frequency encoded imaging. The frequency encoding approach of simultaneous signal acquisition and gradient switching, followed by re-gridding of data points applies additional constraints on the k-space trajectories related to the transition between k-space points [7]. There are similarities between frequency and phase encoded trajectory design, the importance of available gradient slew rate and duty cycle [8], for example, but the nature of phase encoded imaging allows a different approach.

In this paper, we outline a new two-dimensional centric sampling strategy for SPRITE techniques, which can also be used as the basis for a new three-dimensional centric scan sampling scheme. This methodology provides a natural bridge between spiral/conical and radial sampling schemes, but also can be directly used for the generation of over- or under-sampled trajectories. This technique has several natural advantages, but the most valuable are: increased resolution and more robust image contrast, especially in magnetisation preparation methods, which are outlined in this paper.

2. Theory

The aim of MRI imaging is to acquire an NMR signal in the presence of a magnetic field gradient from a certain region of k-space. Therefore, all points within such a region have to be covered in a serial manner. The quality of this signal acquisition is critical and, therefore, we will define several terms related to centric scan acquisitions.

A pattern, by which points are covered, we shall call a *Scheme*. A scheme can be described by its shape, such as Spiral, Radial or Sectoral, for example. We will also refer to an individual realisation of a scheme as a *Trajectory*. Furthermore, a trajectory can be divided into sub-trajectories, which we will call *Leaves*. Generally speaking, in Centric-Scan SPRITE, an individual leaf is a sub-trajectory, which starts at the center of k-space and ends on the periphery. In the case of the Spiral scheme, the leaves have been previously described as *Interleaves* for obvious reasons [4]. We shall avoid this terminology for the sake of consistency. Finally any sequentially sampled part of a leaf, we will call a *Locus*.

There are three principal cases for MRI imaging, when 1, 2 or 3 orthogonal gradients are used, therefore acquiring 1D, 2D or 3D images. In this paper 2D and 3D cases were investigated, since in 1D all families of trajectories devolve into the "half k-space" case [9].

The original SPRITE technique is a longitudinal steady-state imaging method [3]. The longitudinal magnetisation is driven towards a dynamic equilibrium by applying a series of low flip angle *RF*-pulses. The equilibrium magnetisation is given by:

$$M_\infty = M_0 \frac{1 - e^{-TR/T_1}}{1 - \cos\alpha e^{-TR/T_1}}, \quad (1)$$

where α is the *RF*-pulse flip angle; TR is the time between *RF*-pulses. The extent of image blurring is determined by the ratio of the initial (M_0) and equilibrium (M_∞) magnetisations and the rate of transition between them. This particular aspect of SPRITE has been investigated experimentally and analytically by Mastikhin et al. [6] and Prado et al. [10]. The approach to steady state through application of multiple *RF* pulses has been described by Vlaardingerbroek and den Boer [11].

Previous Centric-Scan SPRITE sequences have been based on an Archimedean spiral trajectory (see Fig. 1) To simplify the Fourier transformation, the Archimedean spiral was sampled on a Cartesian grid in k-space. A detailed investigation of this procedure can be found in [4,5] and an example of such a spiral is shown in Fig. 4A. The next step in optimising such a scheme is to create an interleaved spiral sampling of k-space. This approach has been described in detail also in [4]; a representative example

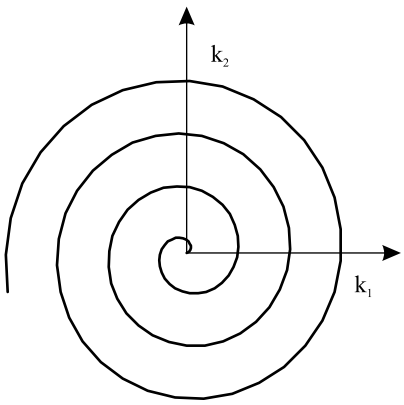

Fig. 1. An illustration of the Archimedean spiral k-space trajectory.

is demonstrated in Fig. 4B. Conical trajectories are a natural extension of interleaved spirals to 3D [4].

2.1. 2D Spiral-like optimised trajectories

Our traditional approach to centric scan trajectories was based on the use of a mathematically preconceived curve, such as the Archimedean spiral, to act as a template in the choice of discrete k-space data points. As a result some k-space data points were omitted, and some were sampled several times. An additional processing step was required to accept or reject duplicate k-space data points on the final trajectory (leaves). The traditional approach was heuristically appealing based, as it was, on a mathematical function.

In this work, we shift to an algorithm driven approach which naturally selects the order of k-space data points according to a simple set of logical rules. These rules are as follows:

- A trajectory starts from the center of k-space.
- A trajectory finishes on a certain ring, the radius of which is determined by the desired resolution in the final image (see Eq. (2)).
- A point with greater radius (a distance to the center of k-space) should not be sampled earlier than a point with smaller radius on the same leaf.
- All points are sampled at least once (the center of k-space is sampled by each leaf).

We justify the form of this algorithm for its simplicity and consistency in sampling separate parts of k-space one at a time (see Section 2.2). To demonstrate the algorithm, we will start with a 1-leaf example of a spiral-like trajectory. First of all, we decide which points must be sampled. All points outside a k-space-centered circle, the radius of which determines the resolution in the final image, are eliminated first.

$$k_{\mathrm{R}} = G_{\max} t_p = \frac{2\pi}{\gamma \Delta r}, \tag{2}$$

where k_{R} is the radius of the chosen k-space circle, $G_{\max}$ is the maximum amplitude of the magnetic field gradient and Δr is the pixel size (assuming isotropic resolution).

One point of the outer ring of such a circle is selected (Fig. 2A). The next point in the sequence would be the adjacent unsampled point with the greatest radius in the clockwise direction (Fig. 2A). It should also be noticed that the clockwise direction is an arbitrary choice. The next step is the same—the point on the outer ring, nearest to the second point is selected. Since each point should be covered only once, every time a point joins the sequence, it is excluded from further accounting. The nearest-point-search procedure is continued until the center of k-space is reached. The order of points in the sequence is then reversed to yield a trajectory (Fig. 2B) that clearly fulfills the requirements detailed above.

To divide a trajectory into N leaves, we can use the same algorithm, but we shall choose N initial points, equally spaced around the periphery of the k-space circle. The 2nd point for each leaf is selected from the common pool of uncovered points; then the 3rd point for each leaf and so on (Fig. 2C). Individual leaves are constructed one point at a time in strict rotation, but using the common pool of uncovered points. As soon as an individual leaf reaches the center of k-space, it is marked as "finished" and excluded from further construction. The procedure continues until all desired k-space data points are assigned to individual leaves. The order of points in all leaves should be reversed in order to start from the center of k-space (Fig. 2C).

This algorithm is difficult to extend into three dimensions. Therefore, different extendable two-dimensional trajectories are required.

2.2. 2D Sectoral-SPRITE trajectories

In creating Sectoral SPRITE trajectories, our approach is slightly different from the creation of Spiral trajectories. Although the first step is again to decide which k-space points have to be covered, the emphasis is no longer placed upon the choice of locus through k-space, but rather upon the division of k-space into logical ensembles, which can themselves be sampled systematically. These ensembles may be divided into smaller sub-ensembles, if necessary, until a simple locus can be constructed from points in each of the smallest sub-ensembles. This approach results in a 2D sampling scheme which may be naturally extended to 3D. It also follows logically from the use of SPRITE sequences to image prepared sample magnetisation where a division of k-space is often necessitated by the sample T_1 or where a segmented k-space acquisition is required due to simple longitudinal magnetisation evolution [5].

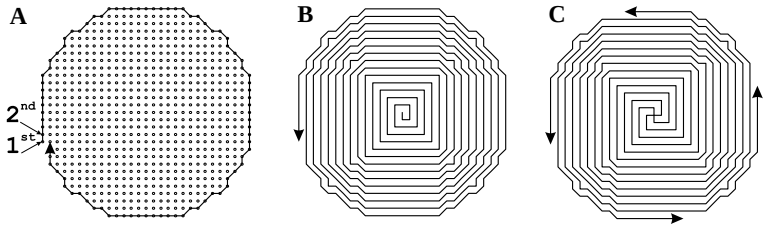

Fig. 2. Construction of 2D Spiral-like trajectories: (A) the first loop of a 1-leaf trajectory; (B) a completed 1-leaf trajectory; (C) a 4-leaf trajectory.

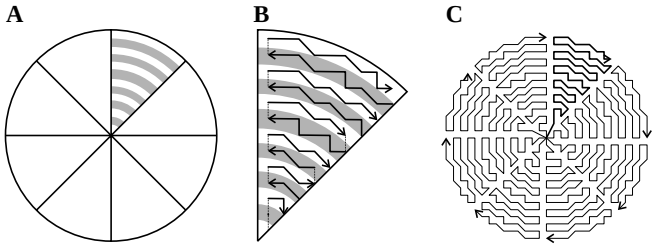

Fig. 3. Construction of representative 2D Sectoral trajectories: (A) The *k*-space circle is divided into 8 sectors; each sector is then divided into "integer" arcs. (B) The points of each arc are connected into a locus, then loci are connected one to another. (C) The final appearance of an 8-leaf Sectoral trajectory.

The primary division of the *k*-space circle is naturally based upon the polar angle. Each leaf consists of an ensemble of points lying in a sector of the *k*-space circle (Fig. 3A).

In the second division, the sub-ensembles will consist of points with equal radius—the distance to the centre of *k*-space. Therefore, each *k*-space sector is divided into "integer" arcs (Fig. 3A), which will be sampled in a serial manner starting from the centre of *k*-space. Inside each arc, a locus can be constructed based on the polar angle of each point (Fig. 3B). The loci can be connected as shown in Fig. 3B. A complete implementation of this procedure is shown as a Sectoral trajectory in Fig. 3C.

A related trajectory, of contemporary but unpublished use in SPRITE imaging [12] is Radial, in which points are sampled along evenly distributed rays. Generalising, we will refer to the number of rays as the number of leaves. Spiral (Fig. 4A) and Radial (Fig. 4B) SPRITE trajectories have in practice been separated by a significant gap in their leaf numbers. Sectoral trajectories can be readily divided into any arbitrary number of leaves, if required. The sectoral sampling strategy logically spans the gap between spiral and radial sampling schemes. An example of the Sectoral trajectory with 32-leaves is displayed in Fig. 4C. Some statistical characteristics of these three schemes can be seen in Table 1.

Table 1
Statistical characteristics of 2D trajectories

	Spiral	Radial	Sectoral
Leaves	1	32	32
Coverage	80.3%	33.3%	99.9%
Average leaf	2564 pts	30 pts	93 pts
Leaf SD	0.0%	16.2%	10.3%

2.3. 3D Sectoral-SPRITE trajectories

The Spiral-SPRITE method can be generalised to three dimensions by changing the gradient in the third spatial direction following the acquisition of a spiral in the transverse plane, creating a cylindrical "stack of spirals" [13]. However, this is only a true centric-scan sequence for the $G_3 = 0$ spiral. A truly centric three-dimensional scan can be undertaken with Conical-SPRITE [4]. One cone of a typical Conical trajectory is represented in Fig. 5. In principle, the number of cones can be arbitrary. However, the current implementation of Conical-SPRITE samples a total of 39 cones, covering approximately 23.5% of the *k*-space data points in a $64 \times 64 \times 64$ cube, which was intentionally done to increase imaging speed.

By replacing each long duration leaf with several shorter ones [4], all beginning at the centre of *k*-space, the leaf duration can be significantly reduced without effecting the overall *k*-space coverage. The interleaved cones are adjusted onto the Cartesian grid and duplicate points between different leaves are removed before they are acquired. This results in a similar sampling density per unit time to that of the 2D Spiral.

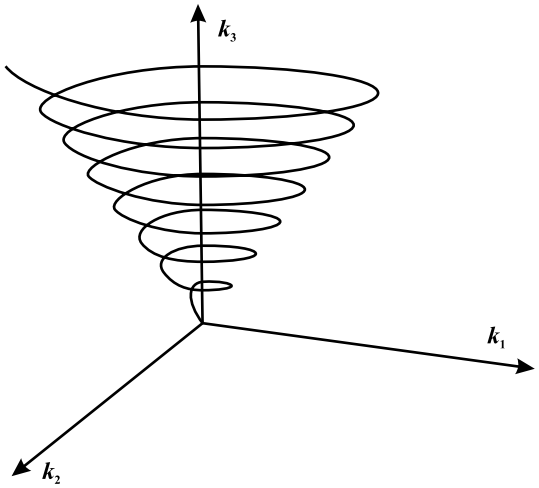

Fig. 5. One cone of a Conical-SPRITE sampling trajectory.

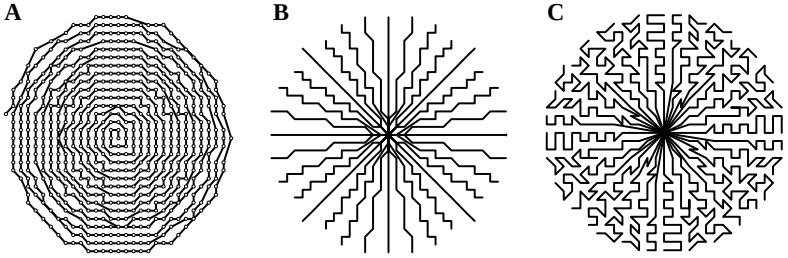

Fig. 4. Two-dimensional SPRITE trajectories: (A) 1-leaf Spiral; (B) 32-leaf Radial; and (C) 32-leaf Sectoral.

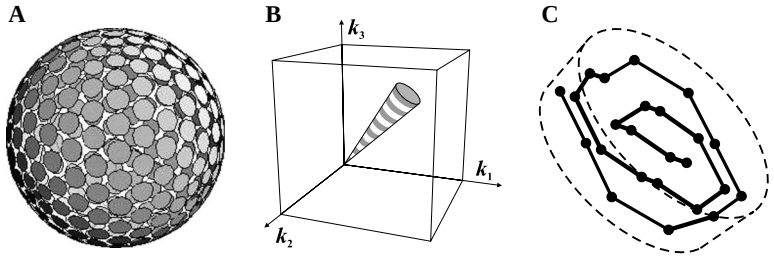

Fig. 6. Construction of 3D Sectoral trajectories: (A) Lebedev set for 2-angle averaging over a full sphere for 302 orientations (courtesy of M. Carravetta and M.H. Levitt, University of Southampton, UK); (B) a solid angle divided into integer pancakes; (C) a Spiral-like locus inside an integer pancake (see Fig. 2).

In this paper, we introduce a new approach to the construction of 3D trajectories based on the same philosophy as the 2D Sectoral-SPRITE method. In the 2D case, the division of a k-space circle into a set of equal sectors is a trivial task. In the 3D case, we shall similarly find a way to divide a k-space sphere into a set of similar solid angles evenly distributed in space. This is a complex task, which requires a separate investigation for optimal results. For our purpose, we will adopt one of the known solutions of the orientations for NMR powder averaging. A number of files, each containing the angular polar coordinates for the centres of evenly distributed solid angles were provided by Marina Carravetta and Malcolm H. Levitt (University of Southampton, UK) [14]. One Lebedev set of coordinates for 2-angle averaging over a full sphere for 302 orientations is illustrated in Fig. 6A.

Each solid angle, a cone, will represent one leaf of the three-dimensional Sectoral trajectory. The leaf is subdivided into "pancakes" by an integer radius which is the distance from the centre of k-space (Fig. 6B). Points on each pancake are joined together into a spiral-like locus from the outermost point to the central one (Fig. 6C) as detailed above (Fig. 2). In addition, the loci of the pancakes with odd integer distance to the center of k-space will be sequenced from inside to outside, in the opposite sense to loci of the even pancakes, which will be sequenced from outside to inside. This alternation allows individual loci to be connected into one leaf inside a solid angle. Thus, the complete 3D sampling scheme combines the 2D Sectoral SPRITE approach to the partitioning of k-space with our new, formalised point sequence selection of trajectory determination.

2.4. Pulse sequences

Fig. 7 depicts the pulse sequence diagram for a typical Sectoral-SPRITE method. The 2D Sectoral trajectories are similar to those of the Spiral scheme, which also consists of a set of discrete gradient steps. The three-dimensional version of Sectoral-SPRITE pulse sequence is similar to its two-dimensional counterparts, but consists of a set of three orthogonal gradients G_1, G_2, and G_3, which also are stepped in a specific pattern.

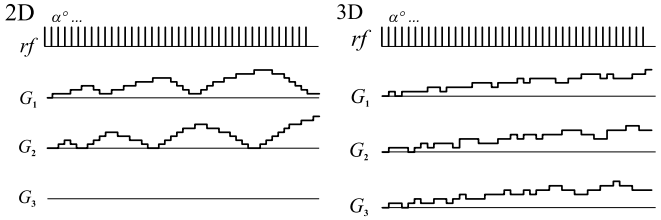

Fig. 7. The 2D Sectoral-SPRITE pulse sequence, where two orthogonal gradients G_1 and G_2 are used. The 3D Sectoral-SPRITE pulse sequence, where three orthogonal gradients G_1, G_2, and G_3 are used. Each gradient step corresponds to a sample excitation using a broadband *RF* pulse with a flip angle α.

3. Results and discussion

A disk shaped cross-linked *cis*-polybutadiene phantom with a variety of geometrical features was imaged as a resolution sample. The geometry and dimensions of the disk are presented in Fig. 8. The bulk lifetimes of the inner cylinder material are $T_1 = 220 \pm 10$ ms, $T_2 = 560 \pm 20$ μs and $T_2^* = 330 \pm 10$ μs. All images were acquired with an encoding time $t_p = 100$ μs, repetition time TR = 0.5 ms and flip angle $\alpha = 3°$. The Fields of View in 2D/3D cases were

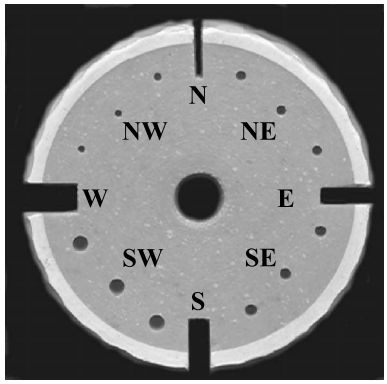

Fig. 8. Cross-linked *cis*-polybutadiene resolution phantom. The outer diameter is 43.0 mm, the outer ring width is 2.5 mm (the outer ring does not appear in any images shown here), the central hole is 6.0 mm. The marked features have the following widths: N = 1.0 mm, E = 2.0 mm, S = 3.0 mm, W = 4.0 mm; diameters: NW = 1.0 mm, NE = 1.25 mm, SE = 1.75 mm, and SW = 2.0 mm.

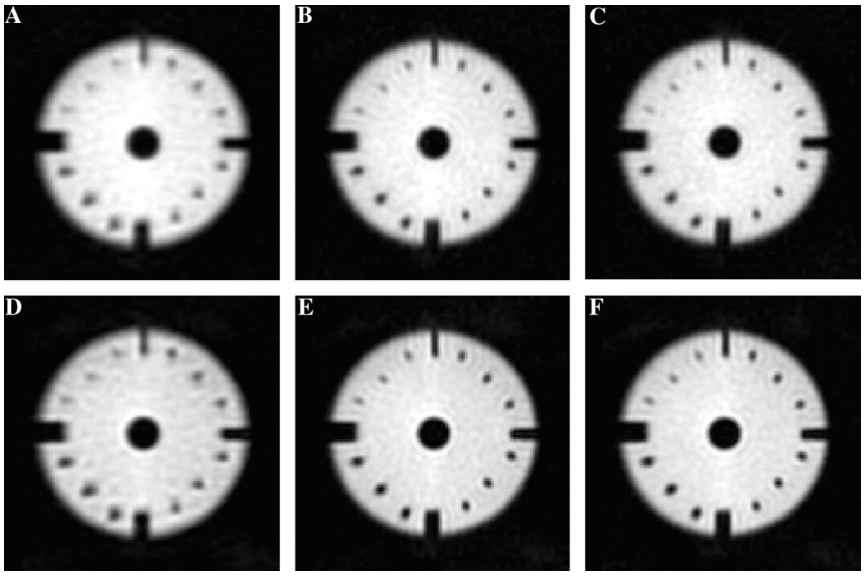

Fig. 9. 2D SPRITE images of the resolution phantom. FOV = 5 cm × 5 cm; matrix 64 × 64. Trajectories: (A) 1-leaf Spiral (trajectory shown in Fig. 4A); (B) 1-leaf Spiral-like (Fig. 2B); (C) 1-leaf Sectoral (Fig. 4D); (D) 8-leaf Spiral (Fig. 4B); (E) 8-leaf Spiral-like; (F) 8-leaf Sectoral (Fig. 4E). The total experimental time for A–C images ≈16 s; for D–F images ≈2 min.

5 cm in each orthogonal direction, with a corresponding spherical matrix dimension of 64 points in diameter. All data sets were zero-filled to 128 points in each dimension of the cubic array before Fourier transformation.

3.1. 2D Sectoral-SPRITE trajectories

Two-dimensional SPRITE images of a resolution phantom are demonstrated in Fig. 9. The Spiral-SPRITE sequence with 1 and 8 leaves was used to acquire the images in Figs. 9A and D. They can be directly compared with images acquired using the Spiral-like (Figs. 9B and E), and Sectoral (Figs. 9C and F) trajectories with 1 and 8 leaves, respectively. All images were acquired with 16 averages. The total experimental time was

$$t_{\mathrm{exp}} \approx [n_{\mathrm{pts}} \times \mathrm{TR} + N \times t_{\mathrm{sep}}] \times n_{\mathrm{ave}}, \quad (3)$$

where n_{pts} is the a number of acquired points; TR is the repetition time; N is a number of leaves; t_{sep} is the time delay between individual leaves; n_{ave} is a number of averages. For the images in Fig. 9 t_{exp} is about 16 s. for 1-leaf, and about 2 min for 8-leaf trajectories. From Fig. 9, we can see that images acquired with Spiral-like and Sectoral trajectories have comparable quality and resolution, while their Spiral counterparts are slightly poorer in both characteristics. This can be explained by a reduction in the number of covered points—while Spiral-like and Sectoral trajectories encode 100% of points in a k-space-centered circle with a 64 point diameter, the traditional Spiral trajectory covers only about 80%. A slight improvement in quality of the 8-leaf images (Figs. 9D–F) over the 1-leaf images (Figs. 9A–C) can be explained by the improvement (narrowing) of the point-spread function with an increasing number of leaves [5].

Even greater differences in quality and resolution can be observed in case of higher numbers of leaves, where traditional Spirals devolve into Radial trajectories. A typical example can be seen in Fig. 10A, where the Radial-SPRITE sequence (Fig. 4C) was used with 64 leaves. In this case only 62% of points in the k-space circle are covered. Better image quality and resolution can be achieved by acquiring the same number of points, but in a fully sampled k-space-centered circle with a smaller radius (despite the concomitant loss in resolution implied by Eq. (2)). A corresponding example is presented in Fig. 10B, where the image was acquired with a

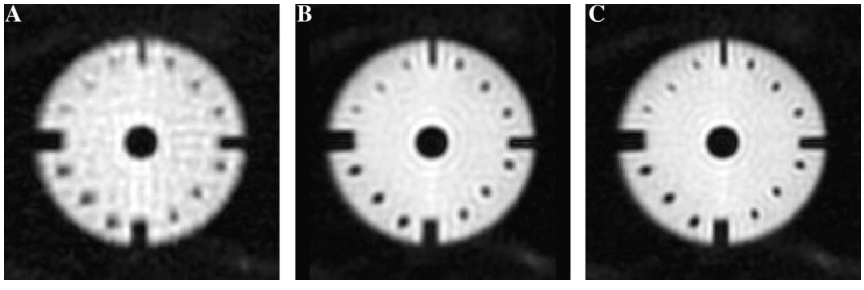

Fig. 10. 2D SPRITE images of the resolution phantom. FOV = 5 cm × 5 cm. (A) 64-leaf Radial trajectory (Fig. 4C), 64 × 64 matrix; (B) 64-leaf Sectoral trajectory, 50 × 50 matrix; (C) 64-leaf Sectoral trajectory, 64 × 64 matrix. The total experimental time for all images ≈17 min.

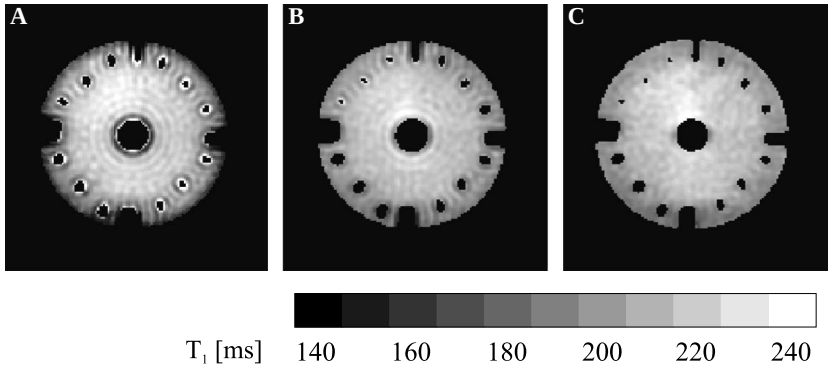

Fig. 11. 2D SPRITE T_1-maps of the resolution phantom. FOV = 5 cm × 5 cm, matrix 64 × 64. Sectoral trajectory: (A) 1-leaf; (B) 8-leaf; (C) 64-leaf. The maps were obtained by inversion recovery preparation of magnetisation followed by a SPRITE readout.

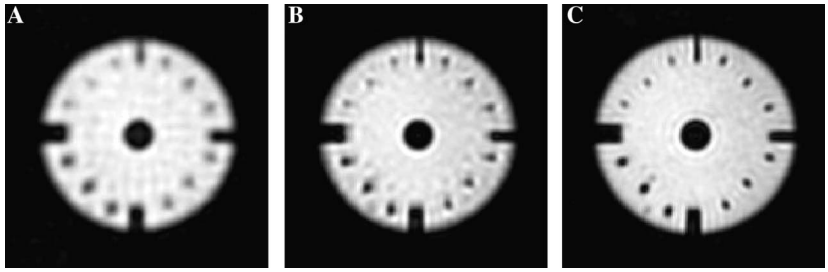

Fig. 12. 2D slices from 3D SPRITE images of the resolution phantom. FOV = 5 cm × 5 cm × 5 cm, matrix 64 × 64 × 64. Trajectories: (A) 1026-leaf Radial; (B) 1005-leaf Conical; (C) 987-leaf Sectoral. The total experimental time for all images ≈67 min.

Table 2
Statistical characteristics of 3D trajectories

	Radial	Conical	Sectoral
Leaves	1026	1005	987
Coverage	26.1%	78.8%	99.9%
Average leaf	37 pts	115 pts	127 pts
Leaf SD	9.9%	15.7%	3.8%

64-leaf Sectoral trajectory but for a 50 × 50 matrix. This image can be directly compared with a "full" 64 × 64 matrix image shown in Fig. 10C, again the 64-leaf Sectoral trajectory was used. All data were zero-filled to 128 × 128 points before Fourier transformation.

In experiments where the imaging part is preceded by some magnetisation preparation, the upper limit of the leaf duration directly depends on the T_1 of the sample. If the leaf duration is longer then T_1—then evolution of sample magnetisation towards a dynamic equilibrium, during k-space sampling, can lead to a variety of artefacts in the final map. A typical example of such artefacts can be observed in a T_1 map itself (Fig. 11). These maps were constructed from SPRITE images preceded by an inversion recovery preparation [6]. An effect known as "edge enhancement" can be clearly identified in Fig. 11A, where the duration of a 1-leaf Sectoral trajectory is significantly longer than the T_1 of the resolution sample. An intuitive guideline for reasonable map quality is that the maximum trajectory length be comparable to or less than T_1. A rigourous treatment of this issue will be the subject of future work. In Fig. 11C, a 64-leaf Sectoral trajectory was used. However, increasing the number of leaves significantly prolongs the total experiment (see Eq. (3)). Some compromise between image quality and the total experimental time has to be found. In this case, such a compromise can be reached by utilising an 8-leaf trajectory. The corresponding T_1 map is demonstrated in Fig. 11B; on the one hand the characteristic features of the resolution sample are clear, on the other hand the image does not suffer from the "edge enhancement" artefact as much as the 1-leaf map.

3.2. 3D Sectoral-SPRITE trajectories

To present three-dimensional Sectoral trajectories, we acquired images of the resolution sample by three different schemes with roughly the same number of leaves. The following schemes were used: Radial, divided into 1026 leaves (rays), standard Conical—1005 leaves (cones), and Sectoral—987 leaves.

The results are presented in Fig. 12. Some statistical characteristics of these three schemes can be seen in Table 2. The noticeable improvement in quality and resolution of the images can be again explained by the increase in the total number of covered points and their locations in the k-space matrix. A narrower distribution of individual leaf lengths, results in lower maximum leaf length. The use of shorter leaves reduces blurring and, therefore, positively contributes to the image resolution, as well as making results of the magnetisation preparation experiments more quantitative.

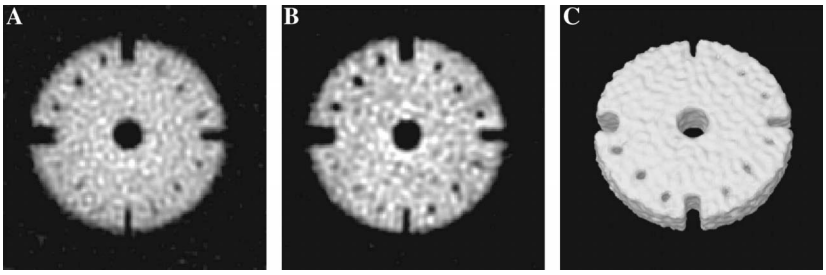

Fig. 13. SPRITE images of the resolution phantom FOV = 5 cm × 5 cm × 5 cm. (A) 2D image, matrix 64 × 64, 1-leaf Sectoral trajectory, total experimental time ≈1.5 s; (B) 2D slice of (C) 3D image, matrix 64 × 64 × 64, 50-leaf 3D Sectoral trajectory, the total experimental time ≈112 s.

3.3. Image quality versus experimental speed

In this final section, we demonstrate some results when the resolution is not the primary consideration, and the experimental time should be minimised. Since the total experimental time for a fixed size matrix depends on many parameters (Eq. (3))—the optimisation of the experiment is a complex task. A detailed investigation of this issue for Spiral and Conical trajectories can be found in [4,5].

Rapidly acquired 2D and 3D images are shown in Fig. 13, where the FOV was set to 5 cm in each orthogonal direction with a 64-point matrix size. The following strategy was used. First we chose the fewest possible number of leaves, which was 1 for the 2D Sectoral trajectory, and 50 for the 3D Sectoral trajectory, with some restrictions necessitated by the gradient duty cycle requirements. Then the shortest possible repetition time (TR) was chosen, 0.5 ms. The main limitation factor in this case is the gradient rise time. In the final step the *RF* pulse flip angle was chosen to be 3°, which was a compromise between *S*/*N* ratio and resolution.

4. Conclusions

The pure phase encode, centric scan, SPRITE technique is well suited to the study of a wide range of short T_2^* systems. Sectoral, Spiral, Radial, and Conical schemes, sample the *k*-space points on a Cartesian grid, which remove the need for any re-gridding procedure prior to image reconstruction. By sampling *k*-space in a more systematic manner, we have significantly improved image quality and resolution in comparison to previous versions. The narrower distribution of individual leaf lengths in the Sectoral scheme, compared to Spiral/Conical trajectories, reduces blurring and makes possible far more robust image contrast produced by magnetisation preparation techniques. The Sectoral SPRITE scheme readily allows the selection of an arbitrary number of leaves without a reduction in *k*-space coverage. This flexibility is critical in the optimisation of magnetisation preparation techniques for a wider range of sample T_1s. Finally, the Sectoral scheme is readily adaptable for future enhancements of the SPRITE technique by the introduction of over- or under-sampling approaches and multiple FID point acquisition.

5. Experimental

All MRI measurements were performed on a MARAN spectrometer (Resonance Instrument, Oxford, UK) equipped with a 7 T wide-bore, horizontal superconducting magnet 7 T/60/AS (Magnex Scientific, Oxford, UK). A standard microimaging gradient set SGRAD156/100/S (Magnex Scientific, Oxford, UK) was used, powered by a set of three power amplifiers 7782 (AE Techron, Elkhart, USA), providing a maximum gradient strength of 0.36 T/m. A home-made 62 mm inner diameter prob was used with a *RF* power amplifier 7T100S (Communication Power, New York, USA). All measurement were carried out at ambient temperature.

The Cartesian components of the Spiral-like and the Sectoral gradient waveforms were constructed using the Prospa (Magritek, Wellington, New Zealand) data processing package. Standard Spiral, Radial, and Conical trajectories were used for comparison [4].

Acknowledgments

The authors thank B. MacMillan and R.P. MacGregor for their technical assistance and M.H. Levitt (University of Southampton, UK) for his help with the orientational angles problem. This work is partly supported by AFMnet, the Advanced Foods and Materials Network of Centres of Excellence. B.J.B. also thanks NSERC of Canada for operating and equipment grants and the Canada Chairs program for a Research Chair in MRI of Materials (2002–2009). B.N. thanks NSERC of Canada for an operating grant. A.A. Kh also thanks A. Jackson (Victoria University of Wellington, New Zealand) for fruitful discussions.

References

[1] S. Emid, J.H.N. Creyghton, High resolution NMR imaging in solids, Physica B and C 128 (1985) 81.
[2] M.D. Robson, D.J. Tyler, S. Neubauer, Ultrashort TE chemical shift imaging (UTE-CSI), Magn. Reson. Med. 53 (2) (2005) 267.
[3] B.J. Balcom, R.P. MacGregor, S.D. Beyea, D.P. Green, R.L. Armstrong, T.W. Bremmer, Single-point ramped imaging with T_1 enhancement (SPRITE), J. Magn. Reson. A 123 (1996) 131.

[4] M. Halse, D.J. Goodyear, B. MacMillan, P. Szomolanyi, D. Matheson, B.J. Balcom, Centric scan SPRITE magnetic resonance imaging, J. Magn. Reson. 165 (2003) 219.
[5] M. Halse, J. Rioux, S. Romanzetti, J. Kaffanke, B. MacMillan, I. Mastikhin, N.J. Shah, E. Aubanel, B.J. Balcom, Centric Scan SPRITE magnetic resonance imaging: optimization of SNR, resolution and relaxation time mapping, J. Magn. Reson. 169 (2004) 102.
[6] I.V. Mastikhin, B.J. Balcom, P.J. Prado, C.B. Kennedy, SPRITE MRI with prepared magnetization and centric *k* space sampling, J. Magn. Reson. 136 (1999) 159.
[7] B.M. Dale, J.S. Lewin, J.L. Duerk, Optimal design of *k*-space trajectories using a multi-objective genetic algorithm, Magn. Reson. Med. 52 (4) (2004) 831.
[8] M. Weiger, K.P. Pruessmann, R. Osterbauer, P. Bornert, P. Boesiger, P. Jezzard, Sensitivity-encoded single-shot spiral imaging for reduced susceptibility artifacts in BOLD fMRI, Magn. Reson. Med. 48 (5) (2002) 860.
[9] I.V. Mastikhin, H. Mullally, B. MacMillan, B.J. Balcom, Water content profiles with a 1D centric SPRITE acquisition, J. Magn. Reson. 156 (2002) 122.
[10] P.J. Prado, B.J. Balcom, I.V. Mastikhin, A.R. Cross, C.B. Kennedy, R.L. Armstrong, A. Logan, Magnetic resonance imaging of gases. A SPRITE study, J. Magn. Resson. 137 (1999) 324.
[11] M.T. Vlaardingerbroek, J.R. den Boer, Magnetic Resonance Imaging, Springer, New York, 1996.
[12] J. Rioux, Non-uniform fast Fourier transformation of SPRITE MRI data, B.Sc. Thesis, University of New Brunswick, 2003.
[13] P. Szomolanyi, D. Goodyear, B.J. Balcom, D. Matheson, SPIRAL-SPRITE: a rapid single point MRI technique for application to porous media, Magn. Reson. Imag. 19 (2001) 423.
[14] M. Edén, M.H. Levitt, Computation of orientational averages in solid state NMR by Gaussian spherical quadrature, J. Magn. Reson. 132 (1998) 220.